SLAC-PUB-14005

Quasi-zero dimensional CuB_2O_4: a resonant inelastic X-ray scattering case study

J. N. Hancock[1], G. Chabot-Couture[2], Y. Li[3], G. A. Petrakovskiĭ[4], K. Ishii[5], I. Jarrige[5], J. Mizuki[5], T. P. Devereaux[1], and M. Greven[1,2]
[1]*Department of Photon Science and Stanford Synchrotron Radiation Laboratory, Stanford, California 94309*
[2]*Department of Applied Physics, Stanford, California 94305*
[3]*Department of Physics, Stanford, California 94305*
[4]*Kirenskiĭ Institute of Physics, Siberian Division, Russian Academy of Sciences, Krasnoyarsk, 660036 Russia and*
[5]*Synchrotron Radiation Research Center, Japan Atomic Energy Agency, Hyogo 679-5148, Japan*
(Dated: September 5, 2008)

We explore the general phenomenology of resonant inelastic scattering (RIXS) using CuB_2O_4, a network of CuO_4 plaquettes electronically isolated by B^{+3} ions. Spectra show a small number of well-separated features, and we exploit the simple electronic structure to explore RIXS phenomenology by developing a calculation which allows for intermediate-state effects ignored in standard approaches. These effects are found to be non-negligible and good correspondence between our model and experiment leads to a simple picture of such phenomenology as the genesis of $d \rightarrow d$ excitations at the K edge and intermediate-state interference effects.

PACS numbers: PACS

New experimental techniques are often born from the advent of new technology, as is the case of resonant inelastic X-ray scattering (RIXS), unique in its atomic species-specific and momentum-selective ability to probe electronic excitations in strongly correlated electron systems[1,2,3,4,5,6,7,8,9,10]. Past work has suggested that RIXS can in principle couple to both local[1,2,10] and extended[3,4,5,6] electronic excitations, including d-d excitations[7,9] and coupled magnetic excitations[11], but detailed quantitative analysis of experimental data has been limited in scope.

In this Letter, we present a comprehensive experimental and theoretical study of the model quasi-zero-dimensional compound CuB_2O_4 that allows us to draw valuable new conclusions about related higher-dimensional compounds and the RIXS technique in general, such as the genesis of $d \rightarrow d$ excitations and intermediate-state effects. These conclusions are made with the aid of data and a novel calculation which explicitly accounts for $4p$ orbital effects, which we find are responsible for previously overlooked RIXS phenomenology. These results present a significant step forward toward making RIXS a quantitative science.

In the type of RIXS of interest here, the resonant condition is met at the Cu K X-ray edge ($1s \rightarrow 4p$ core level transition), which occurs in the hard X-ray regime. A highly localized ($\sim$0.02 Å) $1s$ core hole and a highly extended (bandwidth $\sim$10 eV) $4p$ electron are generated, and the former strongly disturbs the conduction and valence states of the system. The rare decay channels involving the return of the $4p$ electron to the core state constitute resonant elastic (REXS) and inelastic (RIXS) scattering events. The RIXS process is complex, involving strong intermediate-state effects and interfering core-hole decay channels, and simple notions to guide our thinking about this potentially powerful technique are developed below.

CuB_2O_4 consists of covalently bonded CuO_4 subunits isolated electronically by B^{+3} ions, while the Cu retain a nominal +2 valence, as in the high-T_c parent compounds. CuB_2O_4 forms an interesting magnetic phase[12,13] and exhibits a remarkably strong magneto-optical effect[14], but these phenomena occur below 21 K and involve very low-energy (magnetic) degrees of freedom. The X-ray measurements presented here on our flux-grown[12] samples were carried out at room temperature.

Figure 1a shows a $\langle 001 \rangle$ view of part of the crystal structure of CuB_2O_4, which contains two crystallographically inequivalent CuO_4 plaquettes. Figure 1c shows Cu $2p_{\frac{3}{2}}$ and $2p_{\frac{1}{2}}$ X-ray photoemission spectroscopy (XPS) spectra collected on a sample cleaved in-situ under 10^{-8} torr. Each of the four main features is composed of two peaks, with the stronger peak at higher binding energy, and an intensity ratio of about 1:2. The data are well described assuming two sets of four peaks arising from the Cu(1) and Cu(2) sites, respectively, with a shift of $\sim$3.2 eV which could reflect a chemical shift between these sites. In this scenario, XPS signal due to the undistorted Cu(1) sites occurs at lower binding energy. The fit shown in Fig. 1c uses Lorentzian lineshapes and a constant slope plus broad Lorentzian to represent the background. The two peaks within a multiplet (e.g., $2p_{\frac{3}{2}}$) and for one particular site (e.g., Cu(1)) represent the overlap of core hole states with the ground state[15]. The stronger peak at lower binding energy corresponds to the "well-screened" (WS) state with mostly $d^{10}\underline{L}$ character, while the other peak corresponds to the "poorly screened" (PS) state with predominant d^9 character. The splitting between the WS and PS states ($\sim$8 eV) is dominated by the direct repulsion between the core hole and the holes of the valence system. An identification of similar core hole states is possible in the higher dimensional systems, where it is known that nonlocal (inter-plaquette) screening channels play a role[15].

SIMES, SLAC National Accelerator Center, 2575 Sand Hill Road, Menlo Park, CA 94309
Work supported in part by US Department of Energy contract DE-AC02-76SF00515.

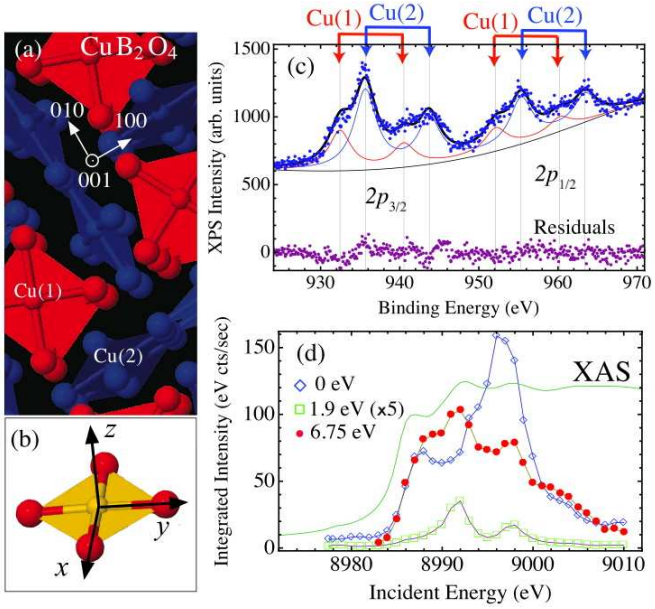

FIG. 1: (Color) (a) Schematic structure of CuB_2O_4, with undistorted Cu(1) plaquettes (red) and distorted Cu(2) plaquettes (blue). B atoms are not shown. (b) Elementary CuO_4 unit and local coordinate system. (c) XPS spectrum. Lines are the result of a fit, descibed in the text. (d) XAS (green line) and integrated RIXS (symbols) intensity versus incident photon energy.

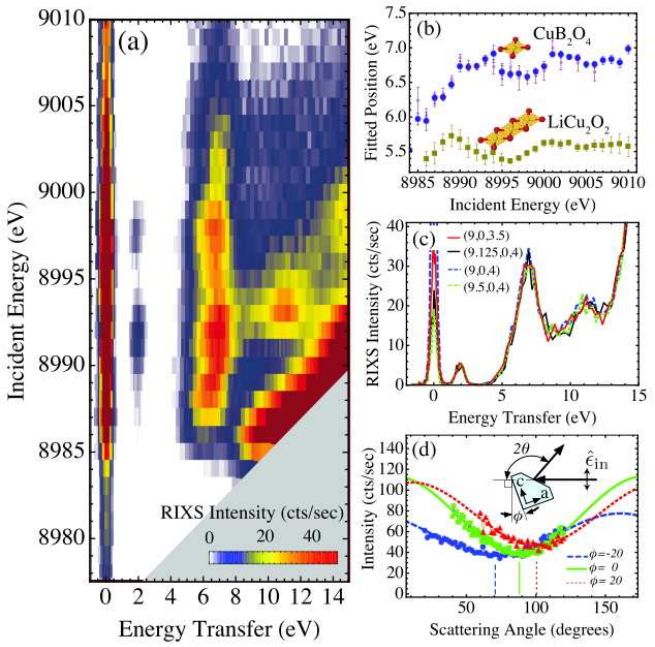

FIG. 2: (Color) (a) False color plot of RIXS spectra taken near $\mathbf{Q}$=(9,0,4) with incident polarization $\hat{\epsilon}_{in}\|[001]$. Spectra were corrected for self absorption using a polarization-dependent mass absorption derived by merging the calculated value with the measured XAS spectra in the region of the edge. This step produces a spectrum which more closely resembles the RIXS cross section, but with systematic errors which are largest when the incident and/or final energy is near the edge at 8985 eV. (b) Incident-energy dependence (∼6-7 eV) for CuB_2O_4 with $\hat{\epsilon}_{in}\|[001]$ (filled circles) and $\hat{\epsilon}_{in}\|[100]$ (open circles). Also shown are data for Li_2CuO_2[18]. (c) Momentum independence of the RIXS spectra for E_{in}=8992 eV. (d) Angle dependence of the MO RIXS signal for three orientations (ϕ) of the crystal (E_{in}=8989 eV and ΔE=6.75 eV). The lines indicate fits to the function $A_0+A_4\cos^2(2\theta-\phi_0)$.

Figure 1d shows X-ray absorption spectroscopy (XAS) data measured through total fluorescence yield with polarization $\hat{\epsilon}_{in}\|[001]$. The large step in the absorption occurs due to dipole transitions that involve the creation of a 1s core hole as the energy is raised through the absorption edge (∼8985 eV). This spectrum reflects the (unoccupied) 4p density of states, but like the XPS spectrum where a 2p core hole was created (Fig. 1c), it also contains information about the response of the valence electrons to the spontaneous formation of the core hole[15,16,17].

Figure 2a shows RIXS spectra taken at the JAEA beamline BL11XU at SPring8 in a horizontal scattering geometry with the incident (horizontal) beam polarization along the tetragonal c axis, near (9,0,4)[24], with scattering angle 2θ∼93°, ϕ∼0 (see Fig. 2d inset). The overall energy resolution was around 380 meV. Several features appear as a function of transferred energy, and their resonance profiles show qualitative differences. The strongest feature is the elastic line, which has a complex energy dependence reflecting resonant phenomena as well as structural information. The second strongest feature appears as a diagonal line and corresponds to a constant scattered photon energy of ∼8976 eV. This fluorescence feature is the $K\beta_{2,5}$ emission line, which is well understood to arise from processes including 3d→1s radiative transitions.

Several other prominent features having Raman-Stokes dispersion appear at about 1.9, 6.8, and 10.9 eV. The 1.9 eV feature resonates at 8992 and 8998 eV, has a resolution limited width, and is stronger than any similar feature reported previously[18]. Higher-dimensional insulating systems (1D[18], 2D[3], 3D[19]) exhibit a charge-transfer excitation near 2 eV. However, for CuB_2O_4 such a non-local process is expected to be absent due to the lack of electronically connected neighboring plaquettes. We suggest that the 1.9 eV feature therefore represents a local Cu d→d excitation, corroborated by our modeling (see below).

In accord with previous work[18,20], we assign the majority of the spectral weight of the prominent ∼ 6.8 eV feature to the molecular orbital (MO) excitation. Contrary to the d→d excitation, which resonates markedly only near 8992 eV and 8998 eV, the MO excitation forms a long streak with an incident-energy dependent center position (Fig. 2b). Similar changes in the position of this inelastic feature were seen also in the edge-shared

cuprate Li_2CuO_2. For CuB_2O_4, we furthermore observe a strong decrease at low incident photon energy that is reminiscent of an avoided level crossing (with the $K\beta_{2,5}$ fluorescence feature).

Figure 2c shows line scans of the RIXS intensity corresponding to several different momentum transfers, demonstrating the nondispersive (i. e. local) character of these excitations and corroborating our classification of CuB_2O_4 as a quasi-zero dimensional system. As a result, we are presented the opportunity to measure the angle dependence of RIXS scattering, shown in Fig. 2d, with angles defined in the inset. We see that the scattering intensity is minimum in the direction of the c axis, suggesting the RIXS scattering intensity is influenced by the crystal orientation, perhaps due to $4p$ electronic effects.

The peak at ∼10.9 eV in Fig. 2a resonates most strongly at 8993 eV. Features in this high energy region might, in principle, be associated with the boron atom, the Mott-Hubbard interaction of the Cu-O subsystem[15], or resonances associated with the Cu $4p$ electrons. In our cluster calculations, described below, we find that RIXS processes with $4p$ final states are the likely origin, as suggested before[10]. In Li_2CuO_2[16,18], a 7.6 eV feature is seen experimentally, but is not accounted for in a model with a limited $4p$ treatment. We suggest that this feature is a $4p$ final states, which can be accounted for in a model akin to our complete model, presented below.

In order to develop a better understanding of our data, we first describe the salient features of a simple cluster calculation involving only two states of a Cu-O plaquette[15]: the Cu $3d_{x^2-y^2}$ ($|d^9\rangle$) and the x^2-y^2 combination of O $2p_\sigma$ orbitals surrounding the central Cu atom ($|d^{10}\underline{L}\rangle$). These two states are shown with black arrows in Figure 3b. When the hybridization t_{pd} is turned on, these bare levels are mixed and the new ground state is formed as a bonding combination of the two basis states: $|g\rangle$=cos $\theta|d^{10}\underline{L}\rangle$+sin $\theta|d^9\rangle$. The antibonding state orthogonal to $|g\rangle$ is referred to as the MO excitation, and these are shown as red arrows in Figure 3b. When a core hole is created through dipolar absorption, this strong perturbing influence gives rise to two new states: $|WS\rangle$=cos $\phi|d^{10}\underline{L}\rangle$+sin $\phi|d^9\rangle$ and $|PS\rangle$=-sin $\phi|d^{10}\underline{L}\rangle$+cos $\phi|d^9\rangle$ (purple arrows). In an XPS or XAS experiment, the projection of the ground state onto each of these states determines the spectral profile (e.g. $I_{\rm XPS}\propto|\langle WS|g\rangle|^2$). In a resonant scattering experiment (RIXS or REXS), the signal arises from double projections, first from the ground state (g) onto intermediate states (WS or PS), and then back to the lower-energy excited state (MO). In our case, this double projection has a particular property: $\langle MO|WS\rangle\langle WS|g\rangle=-\langle MO|PS\rangle\langle PS|g\rangle$, independent of the hopping or core hole interaction strength. This results in equal contributions to RIXS scattering through each of the two intermediate states into the MO state, leading to a double-peak pattern (Figure 3c). Constructive interference of the scattering through these different intermediate states enhances intensity between the two resonance energies, forming a long vertical streak as seen in Figs. 2a, 3c, and 3d.

Figure 1d shows the integrated intensity of the MO excitation in CuB_2O_4 versus incident energy. Similarly broad incident-energy-dependent MO intensities are also seen in the RIXS spectra of the edge-shared 1D cuprates Li_2CuO_2[18] and $CuGeO_3$[16]. While the $4p$ density of states would have a broadening effect, it is expected[16] to effect all inelastic features similarly. The fact that the spectral weight associated with the MO excitation is distinctly broad suggests that the interference effect discussed above is of particular importance in the case of this local excitation.

Because this simple model is incapable of producing any features not related to the MO excitation, we performed a more complete cluster calculation, now considering all orbitals of the valence system (O $2p_\sigma$, $2p_\pi$, $2p_z$, and Cu $3d$ e_g and t_{2g} orbitals) and 'core' system (Cu $1s$, $4p_x$, $4p_y$, and $4p_z$ orbitals). We used a truncated Hilbert space made of spinless fermion states with zero, one and two holes in the valence system, with respectively zero, one and two electrons in the core system (Cu $1s$, $4p$). The Slater-Koster parameters used are ($pd\sigma$)=1.54 eV, ($pd\pi$)=($pp\sigma$)=1 eV, and ($pp\pi$)=0.3 eV[15] and ($4p2p\sigma$)=3.0 eV, ($4p2p\pi$)=1.5 eV to explore the effects of Cu $4p$-O $2p$ hopping. The charge transfer energy ϵ_d-ϵ_p=4.0 eV, $1s$-$3d$ repulsion Q=8.0 eV, and ($pd\sigma$) were chosen to produce the best agreement with the experimental separation and intensity ratio of the XPS peaks in Figure 1c and the MO excitation energy. The d crystal field energies were $\epsilon_{x^2-y^2}$=0, $\epsilon_{3z^2-r^2}$=-0.8 eV, ϵ_{xy}=-1.38 eV, ϵ_{xz}=ϵ_{yz}=-1.51 eV[7]. Each plaquette has a local tetragonal crystal field splitting $\epsilon_{4p_{x,y}}$-ϵ_{4p_z}=5.56 eV, with ϵ_{4p_z}=8 eV, consistent with the present data set and the polarization-induced K-edge shift seen in high-T_c related materials[21] as well as band structure calculations[22].

With the numerical eigendata solutions of this system, we calculate the RIXS cross section of a group of 12 plaquettes in the experimental geometry of our CuB_2O_4 experiments using the Krämers-Heisenberg cross section:

$$\frac{d^2\sigma}{d\omega d\Omega} \propto \sum_{f,\nu} |\langle f|\mathcal{G}_\nu|g\rangle|^2 \delta(E_f - E_g - \hbar(\omega_{\rm in} - \omega_{\rm sc})) \quad (1)$$

with the scattering operator for final photon polarization component $\nu \in \{\pi, \sigma\}$ given as

$$\mathcal{G}_\nu = \hat{\varepsilon}_{{\rm sc},\nu} \cdot \mathbf{J}^\dagger(\mathbf{k}_{\rm sc}) \sum_i \frac{|i\rangle\langle i|}{E_g + \hbar\omega_{\rm in} - E_i - i\Gamma} \hat{\varepsilon}_{\rm in} \cdot \mathbf{J}(\mathbf{k}_{\rm in}).$$

Here E_i is the energy of state i and $\hbar\omega_{\rm in(sc)}$, $\hat{\varepsilon}_{\rm in(sc},\nu)$, and $\mathbf{k}_{\rm in(sc)}$ are the energy, polarization and momentum of the incident (scattered) photon, respectively. $\mathbf{J}(\mathbf{k})$=$\sum_j -i\nabla_j e^{i\mathbf{k}\cdot\mathbf{R}_j}$ is the momentum dependent current operator, which we evaluate numerically using tabulated Hartree-Fock atomic wavefunctions[23]. The core-hole decay rate Γ is set to 1 eV and the δ function in (1) was replaced by a Gaussian of energy dependent width

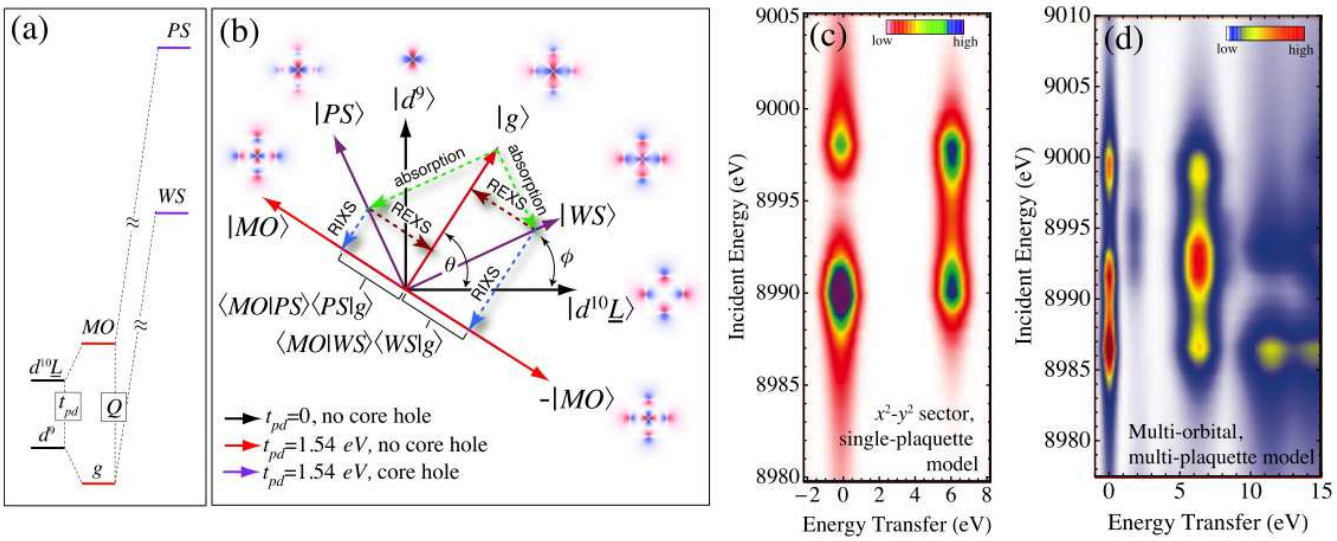

FIG. 3: (Color) (a) Energy level diagram for one CuO_4 plaquette showing bare Cu and O levels, the effect of hybridization t_{pd}, and the effect of a core hole on the Cu site. Each of these three cases are depicted in the x^2-y^2 symmetry Hilbert space in (b). Black lines denote the basis states d^9 and $d^{10}\underline{L}$, red lines denote the eigenstates when t_{pd} is turned on (to 1.54 eV), purple lines indicate the eigenstates with a core hole present (core hole potential Q=8.0 eV). Radiative transitions are denote by dotted arrows for absorption, resonant elastic X-ray scattering (REXS), and resonant inelastic X-ray scattering (RIXS). (c) Calculated RIXS spectrum for the simple CuO_4 plaquette model. (d) Extended calculation of RIXS spectra, including all Cu $3d$ and O $2p$ orbitals, with scattering geometry appropriate to one unit cell of CuB_2O_4 (12 plaquettes).

γ=0.2 eV+0.06 (E_f-E_g) to replicate bandwidth, lifetime, and resolution effects in the computed spectra.

Figure 3d shows the result of the calculation. As in the simpler treatment of Figure 3c, the four-peak pattern associated with the MO and elastic intensities appears, but now in two overlapping sets due to the crystal field splitting of the $4p$ levels, further elongating the vertical streak in the RIXS spectum. In addition, strong features associated with $4p$ electrons in the final state appear at higher energies, similar to the 10.9 eV and higher features and continua including the $K\beta_{2,5}$ fluorescence feature. The features near 2 eV arise from the $3d_{3z^2-r^2}$ crystal field excitation, which is activated by the $4p$-$2p$ hopping, and is extremely weak if $(4p2p\sigma)$=0. This result provides at least a partial explanation for the appearance of $d\rightarrow d$ excitations in RIXS performed at the K edge of copper[9], an effect previously believed to be negligibly weak.

In summary, we have presented XPS, XAS, and RIXS measurements of CuB_2O_4. The combined experimental and cluster model study of the relatively simple system CuB_2O_4 has allowed us to develop important generalizable notions of the RIXS technique. Some aspects of the data can be interpreted in terms of the x^2-y^2 symmetry states alone, but a more complete description requires considerations of $4p$ electronic effects, including hybridization. We have thus unambiguously identified K-edge $d\rightarrow d$ excitations, $4p$ final states, and have made a connection between the advanced core hole spectroscopic technique of RIXS and model parameters. Effects like these are likely to be present in the previous works[9,18], and shed light on the complexity of the RIXS process.

We would like to acknowledge valuable conversations with G.-H. Gweon, J. Hill, S. Johnston, Y.-J. Kim, B. Moritz, B. S. Shastry, and F. Vernay. This work was supported by the DOE under Contract No. DE-AC02-76SF00515 and by the NSF under Grant No. DMR-0705086.

[1] P. Abbamonte, C. A. Burns, E. D. Isaacs, P. M. Platzman, L. L. Miller, S. W. Cheong, and M. V. Klein, Phys. Rev. Lett. **83**, 860 (1999).
[2] J. P. Hill, C. C. Kao, W. A. L. Caliebe, M. Matsubara, A. Kotani, J. L. Peng, and R. L. Greene, Phys. Rev. Lett. **80**, 4967 (1998).
[3] M. Z. Hasan, E. D. Isaacs, Z. X. Shen, L. L. Miller, K. Tsutsui, T. Tohyama, and S. Maekawa, Science **288**, 1811 (2000).
[4] L. Lu, G. Chabot-Couture, X. Zhao, J. N. Hancock, N. Kaneko, O. P. Vajk, G. Yu, S. Grenier, Y. J. Kim, D. Casa, et al., Phys. Rev. Lett. **95**, 217003 (2005).
[5] L. Lu, J. N. Hancock, G. Chabot-Couture, K. Ishii, O. P. Vajk, G. Yu, J. Mizuki, D. Casa, T. Gog, and M. Greven, Phys. Rev. B **74**, 224509 (2006).
[6] S. Grenier, J. P. Hill, V. Kiryukhin, W. Ku, Y. J. Kim,

K. J. Thomas, S. W. Cheong, Y. Tokura, Y. Tomioka, D. Casa, et al., Phys. Rev. Lett. **94**, 47203 (2005).
[7] G. Ghiringhelli, N. B. Brookes, E. Annese, H. Berger, C. Dallera, M. Grioni, L. Perfetti, A. Tagliaferri, and L. Braicovich, Phys. Rev. Lett. **92**, 117406 (2004).
[8] C. Dallera, M. Grioni, A. Shukla, G. Vanko, J. L. Sarrao, J. P. Rueff, and D. L. Cox, Phys. Rev. Lett. **88**, 196403 (2002).
[9] S. Wakimoto, Y. J. Kim, H. Kim, H. Zhang, T. Gog, and R. J. Birgeneau, Phys. Rev. B **72**, 224508 (2005).
[10] P. M. Platzman and E. D. Isaacs, Phys. Rev. B **57**, 11107 (1998).
[11] J. P. Hill, G. Blumberg, Y. J. Kim, D. S. Ellis, S. Wakimoto, R. J. Birgeneau, S. Komiya, Y. Ando, B. Liang, R. L. Greene, et al., Phys. Rev. B **100**, 97001 (2008).
[12] G. A. Petrakovskii, K. A. Sablina, D. A. Velikanov, A. M. Vorotynov, N. V. Volkov, and A. F. Bovina, Cryst. Rep. **45**, 855 (2000).
[13] B. Roessli, J. Schefer, G. A. Petrakovskii, B. Ouladdiaf, M. Boehm, U. Staub, A. Vorotinov, and L. Bezmaternikh, Phys. Rev. Lett. **86**, 1885 (2001).
[14] M. Saito, K. Taniguchi, and T. Arima, J. Jap. Phys. Soc. **77**, 013705 (2008).
[15] M. A. van Veenendaal, H. Eskes, and G. A. Sawatzky, Phys. Rev. B **47**, 11462 (1993).
[16] F. Vernay, B. Moritz, I. S. Elfimov, J. Geck, D. Hawthorn, T. P. Devereaux, and G. A. Sawatzky, Phys. Rev. B **77**, 104519 (2008).
[17] Y. J. Kim, J. P. Hill, C. A. Burns, S. Wakimoto, R. J. Birgeneau, D. Casa, T. Gog, and C. T. Venkataraman, Phys. Rev. Lett. **89**, 177003 (2002).
[18] Y. J. Kim, J. P. Hill, F. C. Chou, D. Casa, T. Gog, and C. T. Venkataraman, Phys. Rev. B **69**, 155105 (2004).
[19] G. Doring, C. Sternemann, A. Kaprolat, A. Mattila, K. Hamalainen, and W. Schulke, Phys. Rev. B **70**, 085115 (2004).
[20] Y. J. Kim, J. P. Hill, G. D. Gu, F. C. Chou, S. Wakimoto, R. J. Birgeneau, S. Komiya, Y. Ando, N. Motoyama, K. M. Kojima, et al., Phys. Rev. B **70**, 205128 (2004).
[21] J. M. Tranquada, S. M. Heald, W. Kunnmann, A. R. Moodenbaugh, S. L. Qiu, Y. W. Xu, and P. K. Davies, Phys. Rev. B **44**, 5176 (1991).
[22] K.-W. Lee and W. Pickett, personal communication.
[23] J. R. Richardson, R. R. Powell, and W. C. Nieupoort, J. Chem. Phys. **36**, 1057 (1962).
[24] Lattice parameters were found to be a=b=11.484$\mathring{A}$, c=5.620$\mathring{A}$.